Formation of hybrid stars from metastable hadronic stars

Domenico Logoteta, Constança Providência, and Isaac Vidaña
Centro de Física Computacional, Department of Physics, University of Coimbra, PT-3004-516 Coimbra, Portugal
(Received 12 July 2013; revised manuscript received 23 October 2013; published 18 November 2013)

We study the consequences of quark matter nucleation in cold hadronic matter employing three relativistic-mean-field models to describe the hadronic phase and the Nambu-Jona-Lasinio (NJL) model for the quark one. We explore the effect of a vector interaction in the NJL Lagrangian and of a phenomenological bag constant on neutron stars metastability. We delineate the region of parameters of the quark phase that allow for the formation of stable hybrid stars with mass compatible with the almost $2M_\odot$ pulsars PSR J1614-2230 ($1.97 \pm 0.04 M_\odot$) and PSR J0348 + 0432 ($2.01 \pm 0.04 M_\odot$). It is shown, however, that not all hybrid star configurations with $\sim 2M_\odot$ are populated after nucleation.

DOI: 10.1103/PhysRevC.88.055802 PACS number(s): 26.60.Dd, 21.65.Qr, 21.65.Mn

I. INTRODUCTION

During the past decades the study of neutron stars has offered the possibility to investigate various topics of modern physics. Owing to their very large central density (several times larger than normal saturation density) neutron stars represent a natural observatory to study the behavior of the matter under extreme conditions. Along this line, the issue of whether neutron stars may host a deconfined quark phase in their cores is still an open question.

Quark matter nucleation in neutron stars has been studied by many authors in both cold [1–14] and finite-temperature [15–23] hadronic matter, or even in the presence of strong magnetic fields [24,25]. These studies suggested that the nucleation process may play an important role in the emission of γ-ray bursts and supernovae explosions. In most of these works, the hadronic phase was described using phenomenological relativistic-mean-field (RMF) models based on effective Lagrangian densities [26]. Among the different RMF models, one of the most popular parametrizations is that of Glendenning and Moszkowski [27] of the nonlinear Walecka model which has been widely used to study the effect of the hadronic equation of state (EOS) on the nucleation process. In particular, in Ref. [10] the effect of different hyperon couplings on the critical mass and stellar conversion energy was analyzed. It was found that increasing the value of the hyperon coupling constants, the stellar metastability threshold mass, and the value of the critical mass increase, thus making the formation of quark stars less likely. In all these works the MIT bag model [28] was used to describe the deconfined phase. In Ref. [29], two models that contain explicitly the chiral symmetry were applied to describe the quark phase, namely the Nambu-Jona-Lasinio (NJL) model [30] (see also [31,32]) and the chromodielectric model (CDM) [33,34]. It was shown there that it is very difficult to populate the quark star branch using that version of the NJL model and, therefore, all compact stars would give pure hadronic stars in that case. On the contrary, with the CDM, both hadronic and quark star configurations can be formed. Recently, in Ref. [35], was discussed the possibility of quark matter nucleation using the microscopic Brueckner-Hartree-Fock approach to model the hadronic phase, and the three quark matter models cited above to describe the deconfined phase. The maximum neutron-star mass predicted within this study was of $1.62 M_\odot$, quite far from the almost $2M_\odot$ pulsars PSR J1614-2230 ($1.97 \pm 0.04 M_\odot$) [36] and PSR J0348 + 0432 ($2.01 \pm 0.04 M_\odot$) [37], recently measured.

In the present work we investigate the nucleation of quark matter in cold hadronic matter using a hadronic EOS based on three different RMF approaches. We consider the TM1 [38], the TM1-2 [39], and the NL3 [40] models. The TM1 and TM1-2 models satisfy the heavy-ion flow constraints for symmetric matter around densities $2\rho_0$–$3\rho_0$ [41] ($\rho_0 = 0.16$ fm^{-3} being the empirical saturation point of symmetric nuclear matter). NL3, on the contrary, does not satisfy these constraints. However it has been used in Ref. [42] as the hadronic EOS in a scenario that allows for hybrid stars with masses above $2M_\odot$. A hard hadronic EOS seems to be a necessary condition for the existence of massive hybrid stars. Although it is well known that hyperons are expected to appear in the neutron-star interior at densities $\sim 2\rho_0$–$3\rho_0$ and play a decisive role for several properties of such objects, we ignore them in this work because, as mentioned in the Abstract, we are mostly interested in the study of the role of the vector interaction and the phenomenological bag constant in the NJL model, and on the determination whether the quark star branch may be populated.

For the quark phase we employ the version of the NJL model presented in Ref. [42] but neglecting the superconducting terms. In this way we get an upper bound in our results, because it is generally accepted that superconductivity softens the EOS. In the version of the NJL model of Refs. [42,43], a phenomenological bag constant B^* was introduced to define the location of the deconfinement phase transition. A task of the present work is to delineate the region of parameters of our models that allow for the formation of stable high-mass neutron stars after the nucleation process. For the formation of a hybrid star it is important that the nucleation time of the metastable hadronic star, from which it originates, be smaller than the age of the universe.

II. THE HADRONIC EQUATION OF STATE

As said before, in this work we have used three popular relativistic mean-field models to describe the hadronic phase

of our system, namely the NL3, the TM1, and the TM1-2 models. These models are based on the following Lagrangian density:

$$\begin{aligned}\mathcal{L} = &\sum_N \bar{\psi}_N \Big[\gamma^\mu \Big(i\partial_\mu - g_{\omega N}\omega_\mu - \frac{1}{2}g_{\rho N}\boldsymbol{\tau}\cdot\boldsymbol{\rho}_\mu\Big) \\ &- (m_N - g_{\sigma N}\sigma)\Big]\psi_N + \frac{1}{2}\partial^\mu\sigma\,\partial_\mu\sigma - \frac{1}{2}m_\sigma^2\sigma^2 \\ &+ \frac{1}{2}m_\omega^2\omega^\mu\omega_\mu - \frac{1}{4}\boldsymbol{\rho}^{\mu\nu}\cdot\boldsymbol{\rho}_{\mu\nu} + \frac{1}{2}m_\rho^2\boldsymbol{\rho}^\mu\cdot\boldsymbol{\rho}_\mu \\ &- \frac{1}{3}bm_N(g_{\sigma N}\sigma)^3 - \frac{1}{4}c(g_{\sigma N}\sigma)^4 \\ &- \frac{1}{4}\Omega_{\mu\nu}\Omega^{\mu\nu} + \frac{1}{4!}\xi g_\omega^4(\omega_\mu\omega^\mu)^2 \\ &+ \Lambda_\omega\left(g_\omega^2\omega_\mu\omega^\mu\right)\left(g_\rho^2\boldsymbol{\rho}_\mu\cdot\boldsymbol{\rho}^\mu\right) \\ &+ \sum_{l=e^-,\mu}\bar{\psi}_l(i\gamma^\mu\partial_\mu - m_l)\psi_l, \end{aligned} \tag{1}$$

where the sum is performed over nucleons, ψ_N, represents the corresponding Dirac field, and interactions are mediated by the σ isoscalar-scalar, ω_μ isoscalar-vector, and ρ_μ isovector-vector meson fields. The mesonic field tensors are given by their usual expressions: $\Omega_{\mu\nu} = \partial_\mu\omega_\nu - \partial_\nu\omega_\mu$, $\boldsymbol{\rho}_{\mu\nu} = \partial_\mu\boldsymbol{\rho}_\nu - \partial_\nu\boldsymbol{\rho}_\mu$. The values of nucleon-meson couplings and the other parameters of the Lagrangian are reported in Table I.

In this work we have included just nucleons in the hadronic phase.

We note, however, that hyperons are expected to appear in neutron-star matter at densities of $2\rho_0$–$3\rho_0$. Their presence in neutron stars has been studied by many authors using either phenomenological [27,44] and microscopic [45] approaches since the pioneer work of Ambartsumyan and Saakyan [46]. It is well known that their appearance softens the EOS leading to a substantial reduction of the neutron-star mass. Recently, it has been shown that the inclusion of mesons with hidden strangeness and, particularly, a weak scalar coupling and a strong vector coupling, may give rise to a quite hard EOS allowing for quite massive stars with hyperonic degrees of freedom [39,47]. However, our present knowledge of the hyperon interactions (particularly, the hyperon-hyperon one) is yet not very well constrained by experimental data. Therefore, the result of these works should be taken with care. The results of our calculation without hyperons should be interpreted just as an upper limit for the maximum star mass. If it is not possible to get a $2M_\odot$ neutron star including only nucleonic degrees of freedom in the hadronic phase, then the presence of hyperons most probably will only worsen this situation. Some results including hyperons will be, however, shown for completeness (see discussion below).

The NL3 model contains neither the quartic term in ω nor the nonlinear ω-ρ one. Their respective coefficients ξ and Λ_ω are put to zero in Table I. The NL3 model has the following saturation properties: saturation density, $\rho_0 = 0.148$ fm^{-3}; binding energy, $E/A = -16.30$ MeV; symmetry energy, $J = 37.4$ MeV; incompressibility, $K = 271.76$ MeV; and effective mass, $M^*/M = 0.60$. For the TM1 and the TM1-2 models all the terms in the Lagrangian (1) are nonzero. The quartic term in ω was proposed in Ref. [38] to get a RMF model able to fit the ground-state properties of several nuclei and Dirac-Brueckner-Hartree-Fock calculations at large densities. The nonlinear ω-ρ term is instead needed to get a good value for the slope of the symmetry energy L at saturation density, as suggested in Ref. [48]. The original TM1 model, with $\Lambda_\omega = 0$, predicts a value of $L = 110$ MeV that is too high according to the experimental constraints coming from different nuclear properties, lying close to the upper limit of isospin diffusion in heavy-ion collisions [49]. Taking $\Lambda_\omega = 0.03$ a more reasonable value of $L = 55$ MeV is obtained. The TM1 and the TM1-2 have the same saturation properties: saturation density, $\rho_0 = 0.145$ fm^{-3}; binding energy, $E/A = -16.30$ MeV; symmetry energy, $J = 36.93$ MeV; incompressibility, $K = 281.28$ MeV; and effective mass, $M^*/M = 0.63$.

III. THE QUARK MATTER EQUATION OF STATE

For the description of the high-density quark matter we have employed the NJL Lagrangian, extended to include the t' Hooft interaction term (proportional to K) and the vector interaction (proportional to G_V):

$$\begin{aligned}\mathcal{L}_{NJL} = &\bar{\psi}(i\gamma^\mu\partial_\mu - \hat{m})\psi \\ &+ G_S\sum_{a=0}^{8}[(\bar{\psi}\lambda_a\psi)^2 + (\bar{\psi}i\gamma_5\lambda_a\psi)^2] \\ &- K\{\det{}_f[\bar{\psi}(1+\gamma_5)\psi] + \det{}_f[\bar{\psi}(1-\gamma_5)\psi]\} \\ &- G_V\sum_{a=0}^{8}[(\bar{\psi}\gamma_\mu\lambda_a\psi)^2 + (\bar{\psi}\gamma_5\gamma_\mu\lambda_a\psi)^2], \end{aligned} \tag{2}$$

where the quark spinor fields ψ_α carry a flavor ($\alpha = u, d, s$) index, the matrix of quark current masses is given by $\hat{m} = \mathrm{diag}_f(m_u, m_d, m_s)$, λ_a with $a = 1, \ldots, 8$ are the well-known Gell-Mann matrices in the color space, and $\lambda_0 = (2/3)1_f$. At

TABLE I. Coupling constants for the NL3, TM1, and TM1-2 models. For the TM1 and TM1-2 models the value of $\Lambda_\omega = 0.03$ ($L = 55$ MeV) has been considered while for the NL3 model no ω-ρ has been included, being, therefore, $\Lambda_\omega = 0$ ($L = 118$ MeV) in this case.

Model	$(\frac{g_\sigma}{m_\sigma})^2$ (fm)^2	$(\frac{g_\omega}{m_\omega})^2$ (fm)^2	$(\frac{g_\rho}{m_\rho})^2$ (fm)^2	b	c	ξ
NL3	15.737	10.523	1.338	0.002 055	−0.002 651	0.0
TM1	15.0125	10.1187	5.6434	0.001 450	0.000 044	0.016
TM1-2	14.9065	9.9356	5.6434	0.001 690	−0.000 797	0.011

zero temperature the pressure is given by

$$p = \frac{1}{2\pi^2}\sum_{i=u,d,s}\int_0^{\Lambda} dk k^2|\epsilon_i| - 2G_s\sum_{i=u,d,s}\sigma_i^2 + 4K\sigma_u\sigma_d\sigma_s - 2G_V\sum_{i=u,d,s} n_i^2 - B_0 - B^* + \sum_{l=e^-,\mu^-} p_l, \tag{3}$$

where ϵ_i are the quasiparticle spectra of quarks, σ_i are quark condensates, n_i are quark number densities, p_l is the lepton pressure, B_0 is the vacuum pressure, and B^* is an effective bag constant. The quark chemical potentials are modified by the vector fields as follows: $\mu_i^* = \mu_i - 4G_V n_i$. The numerical values of the parameters of the Lagrangian are $m_{u,d} = 5.5$ MeV, $m_s = 140.7$ MeV, $\Lambda = 602.3$ MeV, $G_S\Lambda^2 = 1.835$, $K\Lambda^5 = 12.36$.

IV. QUARK MATTER NUCLEATION IN HADRONIC STARS

In bulk matter the hadron-quark mixed phase begins at the "static transition point," defined according to the Gibbs criterion for phase equilibrium:

$$\mu_H = \mu_Q \equiv \mu_0, \quad P_H(\mu_0) = P_Q(\mu_0) \equiv P_0, \tag{4}$$

where

$$\mu_H = \frac{\epsilon_H + P_H}{n_H}, \quad \mu_Q = \frac{\epsilon_Q + P_Q}{n_Q}, \tag{5}$$

are the Gibbs energies per baryon (i.e., average chemical potentials) for the hadron (H) and quark (Q) phases, respectively, and the quantities $\epsilon_H(\epsilon_Q)$, $P_H(P_Q)$, and $n_H(n_Q)$ denote, respectively, the total (i.e., including leptonic contributions), energy density, total pressure, and baryon number density of the two phases. The deconfinement transition in the high-density region relevant for neutron stars is assumed to be of first order. The pressure P_0 defines the transition pressure. For pressures above P_0 the hadronic phase is metastable, and the stable quark phase will appear as a result of a nucleation process. The time scale of the deconfinement transition is determined by the strong interaction and, therefore, quark flavor must be conserved during the deconfinement transition. We call Q^* phase the deconfined quark matter, in which the flavor content is equal to that of the β-stable hadronic phase at the same pressure and temperature. Owing to the weak interaction the flavor content of the deconfined droplet will soon change after deconfinement, and a droplet of β-stable quark matter is formed. Once the first seed of quark matter is formed the pure hadronic star will "decay" into an hybrid or a quark star [50–52]. It was shown in Refs. [3–6,8–11] that pure hadronic stars with values of the central pressure, P_c, larger than P_0 are metastable, and that their mean lifetime depend dramatically on P_c. As in Refs. [3–5], in this work, we define the critical mass $M_{\rm cr}$ of cold and deleptonized stars as the value of the gravitational mass of the metastable hadronic star for which the nucleation time τ is $\sim$1 yr.

The nucleation process of quark matter in hadronic stars can proceed via both quantum tunneling (at zero or finite temperature) and thermal activation [21]. In the present work we only consider cold stellar matter, and, therefore, nucleation only via quantum tunneling. Here we follow closely the formalism presented in Refs. [1,5].

The process of formation of the drop is regulated by its quantum fluctuations in the potential well created from the difference between the energy densities of the hadron and quark phases. Keeping only the volume and the surface terms, the potential well takes the simple form

$$U(\mathcal{R}) = \tfrac{4}{3}\pi n_{Q^*}(\mu_{Q^*} - \mu_H)\mathcal{R}^3 + 4\pi\sigma\mathcal{R}^2, \tag{6}$$

where $\mathcal{R}$ is the radius of the droplet and σ is the surface tension for the surface separating the hadronic phase from the Q^* phase. Within the Wentzel-Kramers-Brillouin (WKB) the quantum nucleation time is equal to

$$\tau_q = (\nu_0 p_0 N_c)^{-1}, \tag{7}$$

where p_0 is the probability of tunneling given by

$$p_0 = \exp\left[-\frac{A(E_0)}{\hbar}\right], \tag{8}$$

where $A(E)$ is the action under the potential barrier, which in a relativistic framework reads

$$A(E) = \frac{2}{c}\int_{\mathcal{R}_-}^{\mathcal{R}_+}\sqrt{[2m(\mathcal{R})c^2 + E - U(\mathcal{R})][U(\mathcal{R}) - E]}\, d\mathcal{R}, \tag{9}$$

$\mathcal{R}_\pm$ being the classical turning points, $m(\mathcal{R}) = 4\pi n_H(1 - n_{Q^*}/n_H)^2\mathcal{R}^2$ the droplet effective mass, and E_0 and ν_0 the ground-state energy and the oscillation frequency of the drop in the potential well $U(\mathcal{R})$, respectively. In Eq. (7) $N_c \sim 10^{48}$ is the number of nucleation centers expected in the innermost part ($r \leqslant R_{\rm nuc} \sim 100$ m) of the hadronic star, where pressure and temperature can be considered constant and equal to their central values.

V. RESULTS AND DISCUSSION

In this section we show the results of our calculations in which we have used the models previously discussed. The model chosen for the hadronic part of our system, our version of the NJL model contains the free parameter B^*, which we have considered as an effective bag pressure, and the coupling of the vector interaction G_V. In addition, the scarce knowledge of the surface tension between the hadronic and the quark phase introduces another parameter, the surface tension σ. Recently, the surface tension of quark matter was calculated within the two-flavor σ model and the two- and three-flavor NJL model [53] and a value in the range 7–30 MeV/fm^2 was obtained. We mostly use values of σ within these range.

A study of finite size effects between the hadronic and the quark phase was also performed in several works [54,55]. The main conclusion of these works is that for large values of the surface tension, namely above 40 MeV/fm^2, the hadron-quark phase transition is closer to a Maxwell than to a Gibbs construction. However, there are still many uncertainties on the approach used to model the hadron-quark phase transition and, as mentioned in Ref. [53], a surface tension in the range 7–30 MeV/fm^2 was obtained. A small surface tension will

bring the whole picture closer to the Gibbs construction. A wide discussion on the advantages and drawbacks in using a Gibbs or a Maxwell construction can be found in Refs. [56–58]. We perform the present discussion within the Gibbs construction. This means that we will be able to obtain hybrid star configurations with both a pure quark phase or a mixed hadronic-quark phase in the star center. Within the Maxwell construction hybrid stars exist only if a pure quark phase exists in the interior. We may expect that the realistic situation lies between both descriptions, and, therefore, we analyze the implications of applying a Maxwell construction in the next section.

In Fig. 1 we show the gravitational mass versus central pressure for various combinations of the three quantities G_V, B^*, σ. For a given EOS, these curves are obtained solving the well-known Tolman-Oppenheimer-Volkov (TOV) [59] equations describing the hydrostatic equilibrium general relativity. Hadronic star sequences are calculated using the NL3 parametrization considering pure nucleonic matter (solid black curve). The hybrid star (YS) sequence is represented by the dashed red curve. The configuration marked with an asterisk represents, in all cases, the hadronic star for which the central pressure is equal to P_0 and thus the quark matter nucleation time is $\tau = \infty$. The critical mass configuration is denoted by a full circle. The final conversion [3–5] of the critical mass configuration into a final quark star with the same stellar baryonic mass is denoted by a solid square. Notice that in most of the cases reported in the figures the quark matter nucleation process will lead to the formation of a black hole (BH).

In all panels of Fig. 1 the blue and black colors refer to the calculation in which the surface tension has been assumed equal to $\sigma = 10$ MeV/fm^2 and $\sigma = 30$ MeV/fm^2, respectively. In this calculation the strength of the vector interaction has been taken as $G_V/G_S = 0.4$, while for the effective bag pressure B^* we have set $B^* = -49.29$ MeV/fm^3 [panels (b) and (d)] and $B^* = -29.5$ MeV/fm^3 [panels (a) and (c)]. For $\sigma = 10$ MeV/fm^2 and $B^* = -49.29$ MeV/fm^3 a stable neutron star can be formed after the nucleation process while, in all the other cases, the final configuration collapses into a BH. The stable final star, obtained using the parameters discussed above, is a neutron star with a pure quark content and not a simple hybrid star with a mixed phase in its core. Similar results are shown in panels (c) and (d) for a calculation in which we put $G_V/G_S = 0$ and we consider $B^* = 0$ MeV/fm^3 [panel (c)] and $B^* = -29.5$ MeV/fm^3 [panel (d)]. In this case all the final configurations are BHs. An equivalent way of presenting these results is shown in Fig. 2, where we plot the evolution of a hadronic star in the gravitational mass (M_G) versus baryonic mass (M_G). In our calculation we assume M_B constant during the nucleation process; therefore, the evolution of neutron stars proceeds on a straight vertical line in this plane.

In Table II we have reported the results of the calculation of the nucleation process using the NL3 EOS; in particular, the following quantities are listed: surface tension (first column), B^* (second column), P_0 (third column), mass of the neutron star with central pressure equal to P_0, $M(P_0)$ (fourth column), critical mass $M_{\rm cr}$ (fifth column), critical baryonic

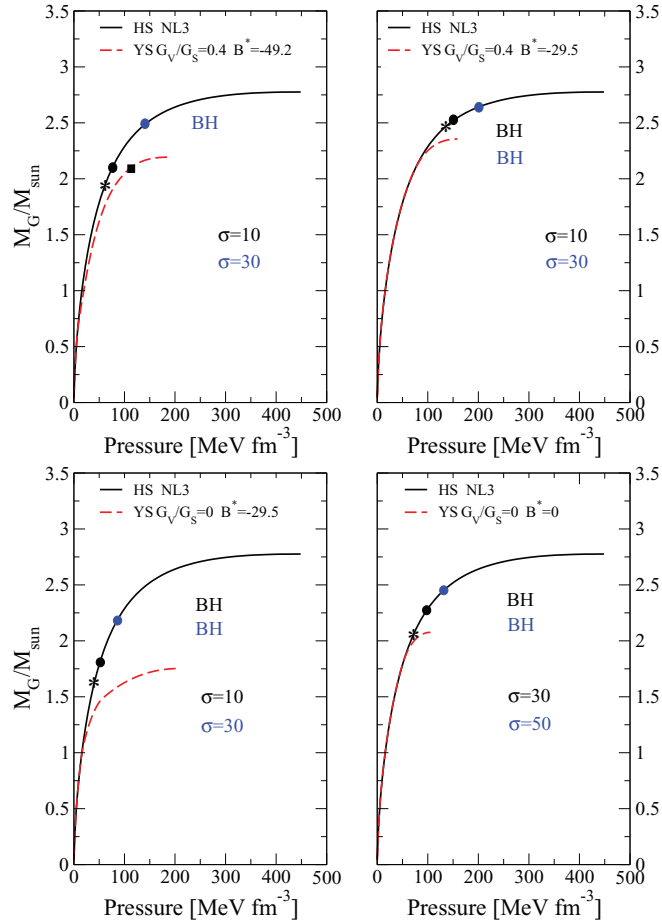

FIG. 1. (Color online) Gravitational mass versus central pressure for compact stars. Hadronic star sequences are calculated using the NL3 parametrization for pure nucleonic matter (black curve). The hybrid star (YS) sequence is represented by the red dashed curve. The quark phase is described by the NJL model with different values of G_V/G_S and B^*. Results are shown for two different surface tensions. The configuration marked with an asterisk represents in all cases the hadronic star for which the central pressure is equal to P_0 and thus the quark matter nucleation time is $\tau = \infty$. The critical mass configuration ($\tau = 1$ yr) is denoted by a solid circle. In panel (a) for $\sigma = 10$ MeV/fm^2, the final quark star mass is denoted by a black square on the YS sequence. In the other cases reported in the figure, the quark matter nucleation process will lead to the formation of a BH.

mass $M^b_{\rm cr}$ (sixth column), final mass $M_{\rm fin}$ (seventh column), and maximum hybrid star mass $M^{\rm YS}_{\rm max}$.

Combining the NJL model without vector interaction ($G_V = 0$) with the NL3 EOS, we note that for $B^* = 0$ and $B^* = -29.59$ MeV/fm^3 the nucleation process leads to the formation of BHs. When we include the vector interaction and we take the largest value of the effective bag constant considered $B^* = -49.23$ MeV/fm^3, we get stable final stars with mass compatible with the $2M_\odot$ pulsar for value of the surface tension between 5 and 15 MeV/fm^2. As we have stated before, a negative B^* enlarges the quark content of the system while the vector interaction goes in the opposite direction. A balance between these two effects is needed to get stable

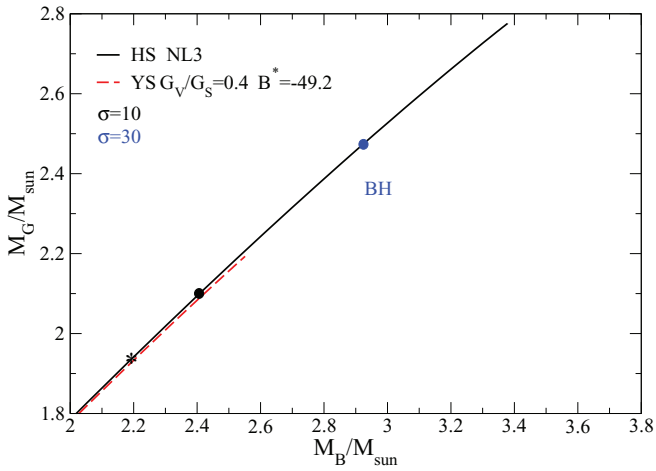

FIG. 2. (Color online) Evolution of a hadronic star in the gravitational-baryonic mass plane using the NJL model with $G_V/G_S = 0.4$ and $B^* = -49.2$ MeV/fm^3 to describe the quark phase, and the NL3 model for the hadronic phase. The (black) line represents the cold hadronic stars (HS) sequence. We consider two different values of the surface tension $\sigma = 10,\ 30$ MeV/fm^2 at the interface between the hadronic and the quark phases. The asterisk and the solid circle on these lines represent the stellar configuration with nucleation time $\tau = \infty$ and the critical mass configuration $\tau =$ 1 yr, respectively. The lower red dashed line represents the cold YS sequence. Assuming M_B constant, the evolution of a neutron star in this plane occurs along a vertical line. For $\sigma = 30$ MeV/fm^2 the nucleation process leads to the formation of a BH.

final stars. The stable final stars obtained using the NL3 EOS are neutron stars with a pure quark content. This calculation improves our previous results of Refs. [29] and [35], where we had found just low-mass hybrid stars as final results of the nucleation process.

However, it is worthwhile to note that although with this model the maximum hybrid star mass can be large ($2M_\odot$) or very large ($2.50M_\odot$) with $G_V = 0$ or $G_V/G_S = 0.4$ and $B^* \leqslant -29.59$ MeV/fm^3, the formation of such massive objects is not possible because the nucleation process leads always, in these cases, to a BH. The radius obtained for the $2.19M_\odot$ neutron star is of 13.2 km. This value is just slightly out of the $M(R)$ constraints found in Refs. [60,61]. Moreover, in Ref. [61] constraints on the slope L have also been imposed and for most of the models considered L should not exceed 65 MeV. Both NL3 and TM1 have a quite high slope L (respectively, 118 and 110 MeV). Including a nonlinear $\omega\rho$ term in the Lagrangian density it is possible to reduce L. A smaller L will give rise to smaller stars still keeping almost unchanged the mass of the maximum mass configuration [39]. All results shown in Table III were obtained with TM1 and its modified TM1-2 including the $\omega\rho$ term for a symmetry energy slope $L = 55$ MeV. All radii are below 12.64 km ($B^* = 0$) and above 11.46 km ($B^* = -39.46$), in good agreement with the constraints of Steiner *et al.* [60,61].

Let us now discuss the results obtained with TM1 and its modified TM1-2 which, as said before, satisfy the constraints obtained in Ref. [41], contrary to NL3. The parametrization TM1-2 has been chosen to be the hardest possible in the range $2\rho_0$–$3\rho_0$ and still satisfy these constraints. The results for these two models combined with the NJL model with $G_V = 0$ and $G_V/G_S = 0.2$ are summarized in Table III. For $G_V = 0$ there are several combinations of parameters that allow the formation of stable hybrid stars, but none of them is able to predict a star with a mass larger than $1.85M_\odot$. The radius of this

TABLE II. The surface tension (σ), the parameter B^*, the transition pressure (P_0), the star mass with a central pressure equal to P_0 [$M(P_0)$], the critical gravitational mass ($M_{\rm cr}$) and baryonic mass ($M^b_{\rm cr}$), the final mass ($M_{\rm fin}$) and the maximum hybrid star mass ($M^{\rm YS}$) obtained for the NL3 hadronic EOS including only nucleons in the hadronic phase, except for the last two lines identified with "NY", which contain hyperons (see discussion in the text). The quark phase is described using the NJL model with and without vector interaction. The maximum quark star mass is the largest mass produced by integrating of the TOV equations and employing the EOS generated by the standard Gibbs construction. In this case the role of the surface tension between the hadronic and the quark phase is neglected.

	σ (MeV/fm^2)	B^* (MeV/fm^3)	P_0 (MeV/fm^3)	$M(P_0)$ ($M_\odot$)	$M_{\rm cr}$ ($M_\odot$)	$M^b_{\rm cr}$ ($M_\odot$)	$M_{\rm fin}$ ($M_\odot$)	$M^{\rm YS}_{\rm max}$ ($M_\odot$)
$G_V = 0$	5	0	91.23	2.19	2.25	2.61	BH	2.07
	10	0	91.23	2.19	2.28	2.66	BH	2.07
	30	0	91.23	2.19	2.43	2.84	BH	2.07
	10	−29.59	38.98	1.59	1.79	2.00	BH	1.75
	30	−29.59	38.98	1.59	2.17	2.51	BH	1.75
$G_V/G_S = 0.4$	5	0	212.75	2.65	2.66	3.21	BH	2.50
	30	0	212.75	2.65	2.71	3.28	BH	2.50
	5	−29.59	135.98	2.46	2.49	2.95	BH	2.35
	30	−29.59	135.98	2.46	2.63	3.10	BH	2.35
	5	−39.46	97.87	2.27	2.33	2.73	BH	2.27
	30	−39.46	97.87	2.27	2.57	3.07	BH	2.27
	5	−49.23	60.35	1.92	2.00	2.27	1.99	2.19
	10	−49.23	60.35	1.92	2.09	2.40	2.08	2.19
	15	−49.23	60.35	1.92	2.20	2.54	2.18	2.19
	30	−49.23	60.35	1.92	2.45	2.89	BH	2.19
$G_V/G_S = 0.4$ NY	5	−39.46	189.93	2.30	2.31	2.70	BH	2.23
$G_V/G_S = 0.2$ NY	9	−49.23	6.81	0.6	2.15	2.48	2.11	2.13

TABLE III. The surface tension (σ), the parameter B^*, the transition pressure (P_0), the star mass with a central pressure equal to P_0 [$M(P_0)$], the critical gravitational mass ($M_{\rm cr}$) and baryonic mass ($M^b_{\rm cr}$), the final mass ($M_{\rm fin}$), and the maximum quark star mass ($M^{\rm YS}$) obtained for the TM1 and TM1-2 hadronic EOS including only nucleons and including a $\omega\rho$ term so that the slope of the symmetry energy is $L = 55$ MeV. The maximum hybrid star mass is the largest mass produced by integrating the TOV equations and employing the EOS generated by the standard Gibbs construction. In this case the role of the surface tension between the hadronic and the quark phase is neglected.

Model	σ (MeV/fm^2)	B^* (MeV/fm^3)	P_0 (MeV/fm^3)	$M(P_0)$ ($M_\odot$)	$M_{\rm cr}$ ($M_\odot$)	$M^b_{\rm cr}$ ($M_\odot$)	$M_{\rm fin}$ ($M_\odot$)	$M^{\rm YS}_{\rm max}$ ($M_\odot$)
TM1 ($G_V = 0$)	5	15.78	257.16	2.11	2.12	2.48	BH	2.00
	5	0	206.72	2.08	2.09	2.44	BH	1.97
	5	−15.78	147.46	1.99	2.02	2.34	BH	1.92
	6	−29.59	82.89	1.75	1.83	2.10	1.83	1.84
	10	−29.59	82.89	1.75	1.88	2.16	BH	1.84
	15	−39.46	26.48	1.10	1.79	2.03	1.78	1.80
	20	−39.46	26.48	1.10	1.93	2.23	BH	1.80
	16	−45.00	6.90	0.48	1.86	2.13	1.83	1.88
	20	−45.00	6.90	0.48	2.02	2.35	BH	1.88
TM1-2 ($G_V = 0$)	5	15.78	206.24	2.18	2.19	2.58	BH	2.07
	5	0	166.69	2.12	2.14	2.50	BH	2.03
	5	−15.78	120.17	2.00	2.03	2.36	BH	1.96
	5	−29.59	69.02	1.72	1.80	2.05	1.80	1.83
	7	−29.59	69.02	1.72	1.83	2.08	1.82	1.83
	10	−29.59	69.02	1.72	1.87	2.14	BH	1.83
	10	−39.46	24.99	1.09	1.56	1.73	1.55	1.80
	17	−39.46	24.99	1.09	1.81	2.06	1.80	1.80
	20	−39.46	24.99	1.09	1.90	2.18	BH	1.80
	18	−45.00	6.89	0.48	1.88	2.15	1.85	1.88
	20	−45.00	6.89	0.48	1.97	2.27	BH	1.88
TM1-2 ($G_V/G_S = 0.2$)	5	−39.46	155.88	2.10	2.14	2.51	BH	2.06
	5	−45.00	82.51	1.82	1.99	2.29	1.98	2.04
	8	−45.00	82.51	1.82	2.04	2.37	2.03	2.04
	10	−45.00	82.51	1.82	2.07	2.42	BH	2.04

last configuration is 11.21 km. Including the vector interaction in the NJL Lagrangian, taking $B^* = -39.46$ MeV/fm^3 and a value of the surface tension around 8 MeV/fm^2, a hybrid star with mass of $2.03M_\odot$ and a radius of 12.41 km is obtained. Just as for the NL3 + NJL model, also with the TM1-2 + NJL model, the quark vector interaction is essential to form a stable high-mass neutron star. For values of $G_V/G_S > 0.2$ we cannot obtain any stable final star configuration using the TM1 and the TM1-2 models. In this case the NJL model vector interaction is so large that it pushes the quark onset to very large densities, inhibiting the nucleation process.

This is indicative of how hard the hadronic EOS needs to be to allow the formation of stars with a mass $\sim 2M_\odot$ with a quark core.

In the last colum of Table III we have reported both for TM1 and TM1-2 models, the maximum neutron-star mass obtained neglecting the finite surface effect at the interface between the hadronic and the quark matter. For the TM1 and the TM1-2 models the largest masses were $M_G = 2.00M_\odot$ ($R = 12.37$ km) and $2.07M_\odot$ ($R = 12.65$ km), respectively. These configurations can be populated if, after nucleation, the star goes through a process of mass accretion.

The above masses have been produced setting $B^* = 15.78$ MeV/fm^3 in both the cases. Larger neutron-star masses can be obtained increasing the value of B^*. However, in all those cases the nucleation process leads to the formation of a BH.

Finally, in Fig. 3 we have delineated the region of the parameters B^* and σ that allow for the formation of stable final stars after quark matter nucleation. Results are shown for the TM1 (red line) and the TM1-2 (blue line) models. Qualitatively similar results have been obtained for the NL3 model, but we do not show them for simplicity. The circles and the squares in the figure have been obtained fixing for each value of B^*, the maximum σ that allows for stable neutron stars after the nucleation process. This means that the combination of parameters that lie in the region under the curves leads to stable final stars while those in the complementary region lead to the formation of BHs. The effect of an effective bag pressure $B^* < 0$ is to lower the onset of the quark phase. This produces an enlargement of the window of metastable stars. To get stable final neutron stars, it is necessary to balance the effect of the surface tension, which delays nucleation and allows for the creation of large massive quark stars, and B^*, which tends to favor a nucleation at low pressures and densities, reducing, therefore, the final maximum mass.

VI. COMMENTS ON THE MAXWELL CONSTRUCTION AND THE INCLUSION OF HYPERONS

In this section we briefly discuss the dependence of the previous results on the approach used to construct the final neutron-star configurations which result from a nucleation

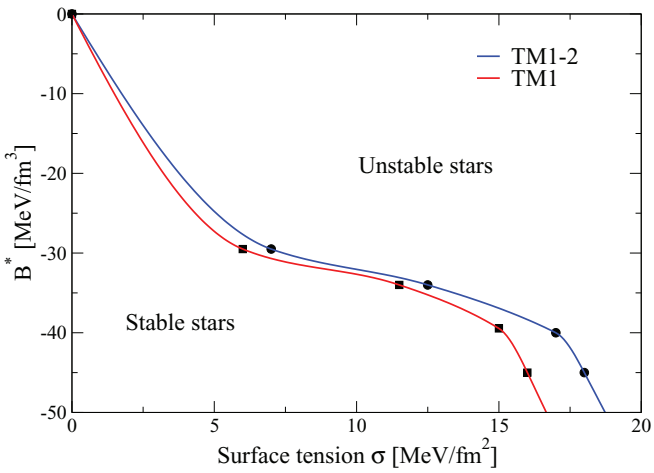

FIG. 3. (Color online) The two curves represent the boundary of the region of parameters that allow for the formation of stable hybrid stars after the nucleation process. The value of the surface tension σ (in MeV/fm^2) is reported on the x axis, while the y axis the value of B^* (in MeV/fm^3) is shown. Results are shown for the TM1 (red line) and the TM1-2 (blue line) models. In the region below the curves stable hybrid stars can be formed as a consequence of the nucleation process, while, in the complementary region, nucleation leads to the creation of BHs.

process. All the calculations shown were performed according to the Gibbs criterion. In the following, we consider another possible approach based on the Maxwell construction. In this case the hadronic and the quark phases are connected by a region with constant pressure, leading, therefore, to a sharp phase transition. Within this phase transition construction possible existing hybrid stars will always have a pure quark core, and, contrary to the Gibbs construction, central cores with mixed hadron-quark matter are excluded.

In Table IV we compare the maximum neutron-star masses and radii obtained using the Maxwell and the Gibbs constructions. For the hadronic phase we have used the TM1-2 model while for the quark phase we have employed the NJL model without vector interaction ($G_V = 0$). We note that the maximum masses produced considering both possibilities are very similar, although the corresponding radii can be quite different in some cases. However, we want to stress that the results of the nucleation process discussed in the previous section for the TM1-2 and the TM1 models are affected only slightly by the choice of adopting the Gibbs instead of the Maxwell construction. In fact, the nucleation process described above takes into account the surface energy and, therefore, the lowest mass configurations of hybrid stars obtained within the Gibbs construction will not be populated because their central pressures lie below the pressure of the critical mass configuration.

The results obtained using the TM1 model are similar to those reported in Table IV and are not shown for brevity.

Using the NL3 model for the hadronic phase, the hybrid stars produced within the Maxwell construction get unstable for $B^* = 0$. A similar result was obtained also in Ref. [56] performing a Maxwell construction with the NJL model but using a different hadronic EOS. Putting $B^* = -29.59$ MeV/fm^3 and $G_V = 0$ a stable hybrid star branch can be obtained. The maximum mass of this sequence is $1.75 M_\odot$ with a radius of 12 km. In this case both the Maxwell and the Gibbs construction give rise to the same hybrid star maximum mass configuration.

We have also studied the effect of including hyperons in the hadronic EOS. As referred above, the hyperon interactions, in particular, the hyperon-hyperon one, are not well constrained. In the following we consider a set of parameters which allows for quite high star masses [39]. We include the meson with hidden strangeness ϕ as in Refs. [39,47], we fix the ω-vector meson couplings according the SU(6) symmetry and the ρ-vector meson couplings according to the hyperon isospin and we fit the couplings of the σ-scalar meson to the hypernuclear potentials in nuclear matter, with $U_\Lambda = -28$ MeV, $U_\Sigma = 30$ MeV, $U_\Xi = 18$ MeV. Taking $B^* = -49.23$ MeV/fm^3 and $\sigma = 9.0$ MeV/fm^2 we obtain the results shown in the last line of Table II with entry NY. In this particular case, it is possible to get a $2.11 M_\odot$ stable hybrid star after nucleation, which includes hyperons. However, as expected, the largest hybrid star configuration is smaller when hyperons are included but not necessarily much smaller if enough repulsion between hyperons exists: Compare the maximum hybrid star mass obtained with $B^* = -39.46$, MeV/fm^3,

TABLE IV. The parameter B^* (second column), the maximum hybrid star masses predicted by the Maxwell (third column), and the Gibbs (fifth column) construction. The corresponding radii are reported in columns four and six, respectively. Results are shown for the TM1-2 hadronic EOS including only nucleons in the hadronic phase with ($\Lambda_\omega = 0.03$) and without ($\Lambda_\omega = 0$) the $\omega\rho$ term. The quark phase is described using the NJL model without vector interaction ($G_V = 0$). The maximum quark star mass is the largest mass produced by integrating the TOV equations and employing the EOS. In this case the role of the surface tension between the hadronic and the quark phase is neglected.

	B^* (MeV/fm^3)	$M_{\rm max}^{\rm YS,\ Maxwell}$ ($M_\odot$)	$R_{\rm max}^{\rm YS,\ Maxwell}$ (km)	$M_{\rm max}^{\rm YS,\ Gibbs}$ ($M_\odot$)	$R_{\rm max}^{\rm YS,\ Gibbs}$ (km)
$\Lambda_\omega = 0.03$	15.78	2.15	12.60	2.07	12.65
	0	2.10	12.72	2.03	12.64
	−15.78	1.99	12.83	1.96	12.58
	−29.56	1.83	11.98	1.83	12.00
$\Lambda_\omega = 0$	15.78	2.15	13.27	2.01	13.19
	0	2.06	13.45	1.95	13.07
	−15.78	1.88	13.53	1.86	12.68
	−29.56	1.75	11.91	1.76	11.89

$G_V/G_S = 0.4$, $\sigma = 5$ MeV/fm^2 with and without hyperons, respectively, $2.23M_\odot$ and $2.27M_\odot$.

VII. SUMMARY AND CONCLUSIONS

In this work we have analyzed the possibility of getting stable high-mass neutron stars, compatible with the recent observation of massive neutron stars, as a consequence of a quark matter nucleation process. We have considered three hadronic matter EOS based on the RMF approach together with a three-flavor NJL model to describe quark matter. The effect on the metastability of hadronic stars of including a vector interaction and a phenomenological bag constant in the NJL model was discussed.

Using the TM1, TM1-2, and NL3 models to describe the hadronic phase, we have shown that it is possible to obtain stable final stars after quark matter nucleation. In particular, to get stable neutron stars, using the NL3 model, it is essential to include the vector term in the NJL Lagrangian density while, for the TM1 and TM1-2 models, the stability of the final star configuration can only be obtained with a weak or zero vector interaction. For the TM1 model, we have obtained slightly less massive stars than the ones predicted by TM1-2 one.

We want to stress that the largest stable final mass obtained with the NL3 model, namely $2.18M_\odot$, is a neutron star containing a quark core while the largest mass predicted by the TM1-2 model, which reads $2.03M_\odot$, is a hybrid star with a central core made of a mixed phase. These values are both compatible with the mass of the pulsars PSR J1614-2230 [36], $1.97 \pm 0.04M_\odot$, and PSR J0348 + 0432 [37], $2.01 \pm 0.04M_\odot$. Note that if after nucleation the star suffers a long-term mass accretion from a companion star in a binary system a star as massive as $2.04M_\odot$ could be achieved within the TM1 parametrization.

According to the calculations performed in this work, the location of the deconfinement phase transition in the phase diagram of QCD, which in our work depends on the hadronic EOS used and the phenomenological bag pressure B^*, plays a very important role on the existence of quark matter in neutron stars. In addition the hadronic part of the system should be sufficiently hard to preserve star stability. It was shown that not all massive quark star configurations are populated after nucleation. In particular, a too large surface tension may originate a BH after nucleation. To have conclusive results, a study of the possibility that nucleation occurs at finite temperature should still be carried out.

The vector interaction in the quark model allows the formation of hybrid stars with a pure quark core; however, this is only possible if the hadronic EOS is very hard. In particular, using an EOS that at intermediate densities was designed to satisfy the upper limit of the constraints obtained in Ref. [41], it is possible to obtain hybrid stars only if no vector interaction or just a weak one is included in the NJL model.

We conclude that more conclusive results depend on a better knowledge of (a) the hadronic EOS at intermediate densities, (b) the surface energy of a quark cluster in a hadronic matter background, and (c) the hyperon interaction.

ACKNOWLEDGMENTS

This work has been partially supported by the initiative QREN financed by the UE/FEDER through the Programme COMPETE under Grant No. SFRH/BD/62353/2009 and the Projects No. PTDC/FIS/113292/2009 and No. CERN/FP/123608/2011 and by NEW COMPSTAR, a COST initiative.

[1] K. Iida and K. Sato, Prog. Theor. Phys. **98**, 277 (1997); Phys. Rev. C **58**, 2538 (1998).
[2] F. Grassi, Astrophys. J. **492**, 263 (1998).
[3] Z. Berezhiani, I. Bombaci, A. Drago, F. Frontera, and A. Lavagno, Nucl. Phys. B Proc. Suppl. **113**, 268 (2002).
[4] Z. Berezhiani, I. Bombaci, A. Drago, F. Frontera, and A. Lavagno, Astrophys. J. **586**, 1250 (2003).
[5] I. Bombaci, I. Parenti, and I. Vidaña, Astrophys. J. **614**, 314 (2004).
[6] A. Drago, A. Lavagno, and G. Pagliara, Phys. Rev. D **69**, 057505 (2004).
[7] T. Harko, K. S. Cheng, and P. S. Tang, Astrophys. J. **608**, 945 (2004).
[8] G. Lugones and I. Bombaci, Phys. Rev. D **72**, 065021 (2005).
[9] I. Bombaci, G. Lugones, and I. Vidaña, Astron. Astrophys. **462**, 1017 (2007).
[10] I. Bombaci, P. K. Panda, C. Providência, and I. Vidaña, Phys. Rev. D **77**, 083002 (2008).
[11] C. Bambi and A. Drago, Astropart. Phys. **29**, 223 (2008).
[12] A. Drago, G. Pagliara, and J. Schaffner-Bielich, J. Phys. G: Nucl. Part. Phys. **35**, 014052 (2008).
[13] L. F. Palhares and E. S. Fraga, Phys. Rev. D **82**, 125018 (2010).
[14] G. Lugones and A. G. Grunfeld, Int. J. Mod. Phys. E **20**, 167 (2011).
[15] J. E. Horvath, O. G. Benvenuto, and H. Vucetich, Phys. Rev. D **45**, 3865 (1992).
[16] J. E. Horvath, Phys. Rev. D **49**, 5590 (1994).
[17] M. L. Olesen and J. Madsen, Phys. Rev. D **49**, 2698 (1994).
[18] H. Heiselberg, arXiv:hep-ph/9501374.
[19] I. Bombaci, D. Logoteta, P. K. Panda, C. Providencia, and I. Vidaña, Phys. Lett. B **680**, 448 (2009).
[20] B. W. Mintz, E. S. Fraga, G. Pagliara, and J. Schaffner-Bielich, Phys. Rev. D **81**, 123012 (2010); B. W. Mintz, E. S. Fraga, J. Schaffner-Bielich, and G. Pagliara, J. Phys. G: Nucl. Part. Phys. **37**, 094066 (2010).
[21] I. Bombaci, D. Logoteta, C. Providencia, and I. Vidaña, Astron. Astrophys. **528**, A71 (2011).
[22] G. Lugones and A. G. Grunfeld, Phys. Rev. D **84**, 085003 (2011).
[23] T. A. S. do Carmo, G. Lugones, and A. G. Grunfeld, J. Phys. G: Nucl. Part. Phys. **40**, 035201 (2013).
[24] S. Chakrabarty, Phys. Rev. D **51**, 4591 (1995).
[25] S. Chakrabarty, Phys. Rev. D **54**, 1306 (1996).
[26] B. D. Serot and J. D. Walecka, Adv. Nucl. Phys. **16**, 1 (1986); Int. J. Mod. Phys. E **6**, 515 (1997).

[27] N. K. Glendenning and S. A. Moszkowski, Phys. Rev. Lett. **67**, 2414 (1991).
[28] E. Farhi and R. L. Jaffe, Phys. Rev. D **30**, 2379 (1984).
[29] D. Logoteta, I. Bombaci, C. Providência, and I. Vidaña, Phys. Rev. D **85**, 023003 (2012).
[30] Y. Nambu and G. Jona-Lasinio, Phys. Rev. **122**, 345 (1961).
[31] M. Buballa, Phys. Rep. **407**, 205 (2005).
[32] D. P. Menezes and C. Providência, Phys. Rev. C **68**, 035804 (2003); M. Baldo, M. Buballa, G. F. Burgio, F. Neumann, M. Oertel, and H.-J. Schulze, Phys. Lett. B **562**, 153 (2003).
[33] H. J. Pirner, G. Chanfray, and O. Nachtmann, Phys. Lett. B **147**, 249 (1984).
[34] J. A. McGovern, M. C. Birse, and D. Spanos, J. Phys. G: Nucl. Part. Phys. **16**, 1561 (1990); W. Broniowski, M. Cibej, M. Kutschera, and M. Rosina, Phys. Rev. D **41**, 285 (1990); S. K. Ghosh and S. C. Phatak, J. Phys. G: Nucl. Part. Phys. **18**, 755 (1992); T. Neuber, M. Fiolhais, K. Goeke, and J. N. Urbano, Nucl. Phys. A **560**, 909 (1993).
[35] D. Logoteta, C. Providencia, I. Vidaña, and I. Bombaci, Phys. Rev. C **85**, 055807 (2012).
[36] P. B. Demorest, T. Pennucci, S. M. Ransom, H. S. E. Roberts, and J. W. T. Hessel, Nature (London) **467**, 1081 (2010).
[37] J. Antoniadis, P. C. C. Freire, N. Wex, T. M. Tauris, R. S. Lynch, M. H. Van Kerkwijk, M. Kramer, C. Bassa *et al.*, Science **340**, 1233232 (2013).
[38] Y. Sugahara and H. Toki, Nucl. Phys. A **579**, 557 (1994).
[39] C. Providencia and A. Rabhi, Phys. Rev. C **87**, 055801 (2013).
[40] G. A. Lalazissis, J. König, and P. Ring, Phys. Rev. C **55**, 540 (1997).
[41] P. Danielewicz, R. Lacey, and W. G. Lynch, Science **298**, 1592 (2002).
[42] L. Bonanno and A. Sedrakian, Astron. Astrophys. **539**, A16 (2012).
[43] G. Pagliara and J. Schaffner-Bielich, Phys. Rev. D **77**, 063004 (2008).
[44] N. K. Glendenning, Astrophys. J. **293**, 470 (1985); F. Weber and M. K. Weigel, Nucl. Phys. A **505**, 779 (1989); J. Schaffner and I. N. Mishustin, Phys. Rev. C **53**, 1416 (1996); S. Balberg and A. Gal, Nucl. Phys. A **625**, 435 (1997).
[45] M. Baldo, G. F. Burgio, and H.-J. Schulze, Phys. Rev. C **58**, 3688 (1998); **61**, 055801 (2000); I. Vidaña, A. Polls, A. Ramos, M. Hjorth-Jensen, and V. G. J. Stoks, *ibid.* **61**, 025802 (2000); I. Vidaña, A. Polls, A. Ramos, L. Engvik, and M. Hjorth-Jensen, Nucl. Phys. A **691**, 443 (2001); H.-J. Schulze, A. Polls, A. Ramos, and I. Vidaña, Phys. Rev. C **73**, 058801 (2006); H. Đapo, B. J. Shaefer, and J. Wambach, *ibid.* **81**, 035803 (2010); H.-J. Schulze and T. Rijken, *ibid.* **84**, 035801 (2011); I. Vidaña, D. Logoteta, C. Providência, A. Polls, and I. Bombaci, Eur. Phys. Lett. **94**, 11002 (2011).
[46] V. A. Ambartsumyan and G. S. Saakyan, Sov. Astron. **4**, 187 (1960).
[47] S. Weissenborn, D. Chatterjee, and J. Schaffner-Bielich, Nucl. Phys. A **881**, 62 (2012); Phys. Rev. C **85**, 065802 (2012).
[48] C. J. Horowitz and J. Piekarewicz, Phys. Rev. C **64**, 062802 (2001).
[49] L. W. Chen, C. M. Ko, and B. A. Li, Phys. Rev. Lett. **94**, 032701 (2005).
[50] A. V. Olinto, Phys. Lett. B **192**, 71 (1987).
[51] H. Heiselberg, G. Baym, and C. J. Pethick, Nucl. Phys. B (Proc. Suppl.) **24**, 144 (1991).
[52] I. Bombaci and B. Datta, Astrophys. J. **530**, L69 (2000).
[53] M. B. Pinto, V. Koch, and J. Randrup, Phys. Rev. C **86**, 025203 (2012).
[54] T. Endo, T. Maruyama, S. Chiba, and T. Tatsumi, Prog. Theor. Phys. **115**, 337 (2006).
[55] T. Maruyama, S. Chiba, H.-J. Schulze, and T. Tatsumi, Phys. Rev. D **76**, 123015 (2007); N. Yasutake, T. Maruyama, and T. Tatsumi, *ibid.* **80**, 123009 (2009).
[56] N. Yasutake and K. Kashiwa, Phys. Rev. D **79**, 043012 (2009).
[57] M. Hempel, G. Pagliara, and J. Schaffner-Bielich, Phys. Rev. D **80**, 125014 (2009); N. Yasutake, T. Noda, H. Sotani, T. Maruyama, and T. Tatsumi, *Recent Advances in Quarks Research* (Nova, Hauppauge, NY, 2013), Chap. 4, p. 63.
[58] A. Bhattacharyya, I. N. Mishustin, and W. Greiner, J. Phys. G: Nucl. Part. Phys. **37**, 025201 (2010).
[59] S. L. Shapiro and S. A. Teukolsky, *Black Holes, White Dwarfs and Neutron Stars* (Wiley, New York, 1983); N. K. Glendenning, *Compact Stars: Nuclear Physics, Particle Physics and General Relativity*, 2nd ed. (Springer, Berlin, 2000); P. Haensel, A. Y. Potekhin, and D. G. Yakovlev, *Neutron Stars 1: Equation of State and Structure* (Astrophysics and Space Science Library, Springer, New York, 2007).
[60] A. W. Steiner, J. M. Lattimer, and E. F. Brown, Astrophys. J. **722**, 33 (2010).
[61] A. W. Steiner, J. M. Lattimer, and E. F. Brown, Astrophys. J. Lett. **765**, L5 (2013).